Grain size effect on the magnetic cluster-glass properties of $La_{0.88}Sr_{0.12}CoO_3$

2010 J. Phys.: Condens. Matter 22 116001

(http://iopscience.iop.org/0953-8984/22/11/116001)

J. Phys.: Condens. Matter **22** (2010) 116001 (8pp) doi:10.1088/0953-8984/22/11/116001

Grain size effect on the magnetic cluster-glass properties of $La_{0.88}Sr_{0.12}CoO_3$

M Patra, S Majumdar and S Giri

Department of Solid State Physics, Indian Association for the Cultivation of Science, Jadavpur, Kolkata 700 032, India

E-mail: sspsg2@iacs.res.in (S Giri)

Received 6 November 2009, in final form 22 January 2010
Published 23 February 2010
Online at stacks.iop.org/JPhysCM/22/116001

Abstract

We report the grain size effect of hole-doped cobaltite, $La_{0.88}Sr_{0.12}CoO_3$, where average sizes are varied from ∼35 to ∼240 nm. The bulk compound is a cluster-glass (CG) compound composed of short range ferromagnetic (FM) clusters embedded in the spin-glass (SG) matrix at low temperature. The short range FM clusters are still retained in the nanocrystalline compound with average size ∼35 nm which are associated with the SG component, displaying CG-like spin dynamics at low temperature. The exchange bias (EB) effect manifested by the shifts in the hysteresis loop is observed due to the field cooling where EB effect is weakened systematically with decreasing grain size. The decrease in the fraction of the FM component is found to be correlated with the weakening of the EB effect with decreasing grain size. Interestingly, the signature of the EB phenomenon due to the field-cooled effect is also evidenced in the temperature as well as the time dependence of resistivity. The grain interior phase separation scenario around the FM/SG interface region has been proposed to interpret the experimental results.

(Some figures in this article are in colour only in the electronic version)

1. Introduction

The hole-doped cobaltites, $R_{1-x}A_xCoO_3$ (R = rare earth and A = divalent ion) having a perovskite structure, are fascinating for the complex magnetoelectric phase separation [1–3]. Analogous to that observed in manganites the cobaltites have been recently shown to exhibit a delicate interplay between charge, spin, orbital and lattice degrees of freedom where an additional degree of freedom, viz. spin state of the Co ion, plays a significant role. The comparable strength of Hund's exchange coupling and the crystal field splitting leads to different accessible spin states, e.g. low spin, intermediate spin and high spin of Co^{3+} in $LaCoO_3$ [4–7]. As a result of hole doping a stable intermediate-spin state of Co^{4+} additionally appears in $La_{1-x}Sr_xCoO_3$, which leads to the spectacular changes in the magnetic, transport and structural properties [1]. The complex magnetic and transport results displaying coexistence of short range ferromagnetic (FM) ordering and a spin-glass (SG) state at low temperature have been proposed by Wu *et al* in the hole-doped cobaltites, $La_{1-x}Sr_xCoO_3$ [1]. At a low doping, semiconducting transport properties have been reported where FM metallic clusters embedded in a non-FM insulating matrix were confirmed by neutron as well as NMR results [8–11]. The low-temperature magnetic properties of a non-FM matrix were realized in the SG or cluster-glass (CG) state [1, 4, 12, 13]. The coexisting FM and glassy magnetic states were proposed even at high doping for $x = 0.5$ [14, 15]. With increasing x the fraction of FM metallic clusters increases while FM clusters coalesce together for $x > 0.18$, leading to an unusual long range FM ordering associated with metallic conductivity in the ordered state. In fact, a metal–insulator transition was coincident with the onset of FM ordering at $x = 0.18$ and conductivity behavior was interpreted in terms of the percolation model [1]. An interesting scenario of intragranular tunneling magnetoresistance has been reported in $La_{1-x}Sr_xCoO_3$ where glassy magnetic behavior in the transport properties was proposed in cobaltites close to the percolation limit of hole doping [9, 16, 17].

Recent reports on nanocrystalline FM and charge-ordered manganites exhibit a variety of unusual behavior in the magnetic and transport properties such as strong surface effect [18, 19], retention of charge-ordered state [20–22], enhancement of FM state and metallic conductivity [23], suppression of phase coexistence [24], size effect on the observed exchange bias phenomenon [25–28], etc. Although few examples of the size effect are observed in manganites, the investigation of the size effect has not been explored adequately in cobaltites. Recently, size-dependent ferromagnetism has been reported, interpreting a different origin of ferromagnetism in nanostructured $LaCoO_3$ [29, 30]. Herein, we investigate the grain size effect on a hole-doped cobaltite, $La_{0.88}Sr_{0.12}CoO_3$. In bulk form the coexistence of short range FM clusters embedded in the SG-like matrix has been realized at low temperature [1, 4, 12, 13]. Recently, fascinating evidence of an exchange bias (EB) effect was reported below the spin freezing temperature in the bulk compound which was attributed to the spontaneous phase separation in the grain interior [31–33]. EB typically manifests itself by the shift in the magnetic hysteresis loop from the origin when the sample has been cooled from high temperature in a static magnetic field [34–36]. The origin of EB is typically attributed to the pinning effect at the FM and antiferromagnetic (AFM) interfaces in a magnetic heterostructure. However, EB has also been observed recently in materials having FM/SG [25, 31–33, 37, 38] and FM/ferrimagnetic [39] interfaces other than the FM/AFM systems.

In this paper, we report the magnetic and transport properties of nanocrystalline $La_{0.88}Sr_{0.12}CoO_3$, where the phase separation scenario in the nanocrystalline compound is compared with the bulk counterpart. The grain size of the compound is varied from ∼35 to ∼240 nm. Interestingly, we observe the signature of the EB phenomenon in the magnetic as well as transport properties where the EB effect is significantly weakened by decreasing the average grain size. The new size-dependent results exhibit contrasting behavior compared to the typical manifestation of the size effect on the EB phenomenon where the effect is weakened with increasing grain size even in the spontaneously phase-separated compounds [25–28]. The grain size dependence of the coexisting phase fraction has been discussed in order to interpret the observed results. AC susceptibility measurements on the compound with average grain size ∼35 nm clearly indicate the CG-like state at low temperature having slower spin dynamics than the bulk counterpart.

2. Experimental details

The polycrystalline compound, $La_{0.88}Sr_{0.12}CoO_3$, was prepared by the sol–gel technique using citrate precursor which was described in our previous report [40]. The as-synthesized gel was initially dried and then heated at 873, 1073 and 1273 K. Average sizes of the compounds are found to be ∼35, ∼135 and ∼240 nm, respectively. The sizes of the particles were confirmed by transmission electron microscopy (TEM) using a microscope, JEOL JEM-2010, and scanning electron microscopy (SEM) using a JEOL FESEM microscope

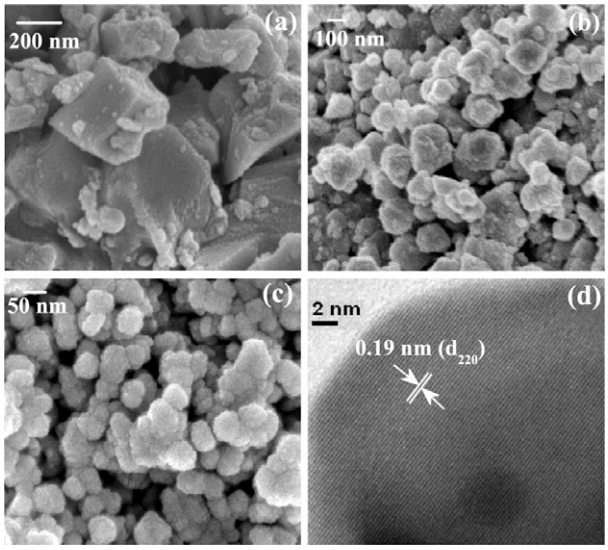

Figure 1. SEM image of (a) S240, (b) S135 and (c) S35. HRTEM image of S35 is shown in (d).

(JSM-6700F). SEM images of the samples having average sizes ∼240, ∼135 and ∼35 nm are shown in figures 1(a), (b) and (c), respectively. Henceforth, we address the samples as S35, S135 and S240 having average grain sizes 35, 135 and 240 nm, respectively. A high resolution TEM (HRTEM) image of S35 is shown in figure 1(d). A single lattice fringe with spacing 0.19 nm is displayed in the figure where the spacing matches exactly with the spacing of the (220) plane estimated from the x-ray diffraction pattern. The single phase of the crystal structure was confirmed by a powder x-ray diffractometer (Seifert XRD 3000P) using Cu Kα radiation. The powder x-ray diffraction patterns are shown in figure 2 which could be indexed by the rhombohedral ($R\bar{3}c$) structure. The lattice parameters are estimated to be $a = 5.382(7)$ Å, 5.399(4) Å and 5.393(1) Å with $\alpha = 60.44(9)$, 60.66(6) and 60.66(2) for S35, S135 and S240, respectively, which indicate that lattice constant as well as the volume of the unit cell remains almost unchanged for S135 and S240 while the volume of the unit cell decreases to ∼1% for S35 compared to S240. The resistivity was measured using the standard van der Pauw technique. Magnetoresistance (MR) was measured using a superconducting magnet system (Cryogenic Ltd., UK). DC magnetization was measured using a commercial superconducting quantum interference device (SQUID) magnetometer (MPMS, evercool). In the case of the zero-field-cooled (ZFC) mode the sample was cooled down to the desired temperature in zero field while for the field-cooled (FC) mode the sample was cooled in a static magnetic field.

3. Experimental results and discussions

3.1. Low-field dc magnetization and ac susceptibility

The ZFC–FC effect of magnetization measured at 200 Oe for S35, S135 and S240 is shown in figure 3. A peak is observed in the ZFC magnetization around ∼55 K (T_p) with a large field-cooled effect while FC and ZFC magnetization

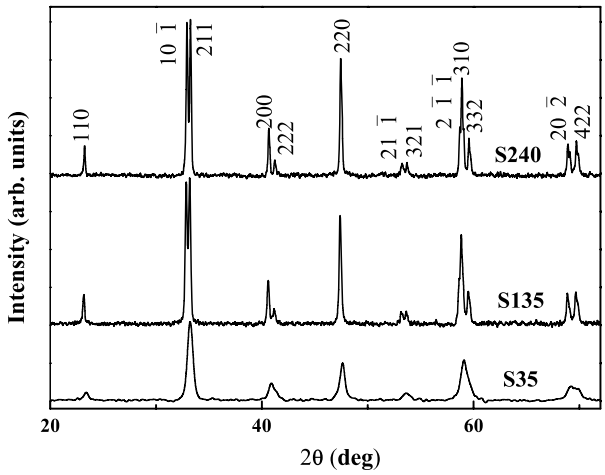

Figure 2. X-ray diffraction patterns of S35, S135 and S240. Peaks are indexed by different planes of the rhombohedral structure.

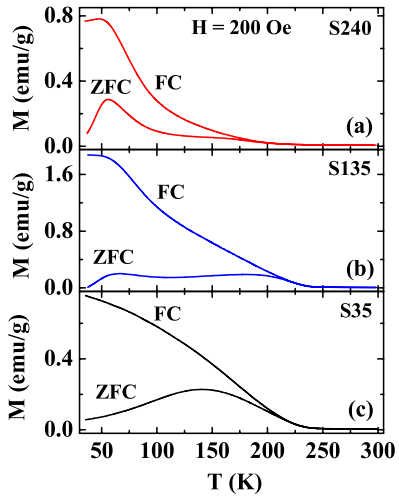

Figure 3. Temperature dependence of the FC–ZFC effect of magnetization for (a) S240, (b) S135 and (c) S35.

deviates from each other below ∼170 K (T_{irr}) for S240. The values of T_p and T_{irr} are in excellent agreement with the phase diagram proposed by Wu *et al* [1]. The peak at T_p is rounded off and shifted towards higher temperature with decreasing grain size. The value of T_p and T_{irr} are ∼65 K and ∼220 K, respectively, for S135. The value of T_{irr} is nearly the same for S135 and S35. The features at T_p and T_{irr} are absent for S35. Instead, a broadened peak (T_f) around ∼140 K is observed in the ZFC magnetization. Temperature variation of ZFC magnetization for S35 is clearly distinct from the results of S135 and S240. The ZFC magnetization for S135 and S240 seems to be consistent with the reported results where T_p behaves like an SG transition temperature [1]. In order to characterize the peak around ∼140 K for S35, temperature variation of ac susceptibility measurements was carried out at five different frequencies (f), viz. 0.12, 1, 10, 100 and 500 Hz, with an ac field = 3 Oe which are shown in figure 4. T_f in $\chi'(T)$ and $\chi''(T)$ increases with f. The value of $\Delta T_f/T_f\Delta(\log\omega)$ primarily characterizes the origin of T_f, where $\omega = 2\pi f$ is the angular frequency. We estimate that the value of $\Delta T_f/T_f\Delta(\log\omega)$ obtained from χ' is ≈ 0.03 which lies in between the ranges for metallic SG (0.005–0.01) and insulating SG (0.06–0.08) compounds [41]. The f dependence of T_f was tested using the phenomenological Vogel–Fulcher (VF) law:

$$\tau = \tau_0 \exp[E_a/k_B(T_f - T_{VF})] \quad (1)$$

where τ, E_a and T_{VF} are the inverse of the measuring frequency, activation energy and VF temperature, respectively [41]. The best fit of T_f from χ' is shown in the inset of figure 4 (left axis). The parameters obtained are E_a/k_B = 140 K and T_{VF} = 22 K. The value of τ_0 is $\sim 10^{-6}$ s, which is much slower than the value ($\sim 10^{-9}$) of typical SG compounds [41]. The other approach to test the glassy magnetic behavior is the standard theory of dynamical scaling near the phase transition at T_f. The conventional result of dynamical scaling relates the critical relaxation time (τ') to the correlation length (ζ) as [41]

$$\tau' = \tau_0'\zeta^{-z\nu} \quad (2)$$

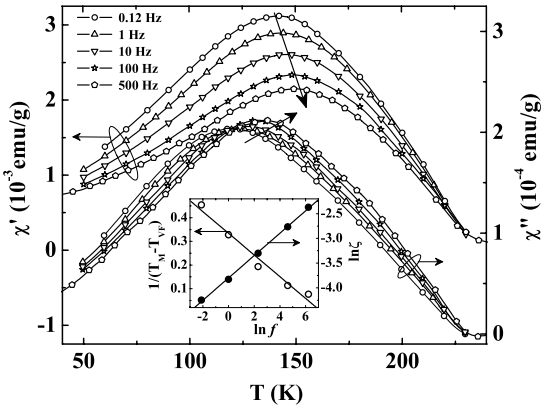

Figure 4. Temperature variation of real, χ' (left axis), and imaginary, χ'' (right axis), part of ac susceptibility at different frequencies (f) for S35. Arrows indicate the increasing direction of f. The inset exhibits the fit using the Vogel–Fulcher law and dynamical scaling.

where $\zeta = (T_f - T_0)/T_0$, τ_0' is the microscopic flipping time, z is the dynamic exponent, ν is the spin-correlation length exponent and T_0 corresponds to the dc value of T_f for $f \to 0$. The best fit is shown in the inset of figure 4 (right axis). The value of T_0 is 140 K, obtained from $\chi'(T)$ which is equal to the temperature at which the peak is observed in the dc magnetization. The values of $z\nu$ and τ_0' are 4.4 and $\sim 10^{-9}$ s, respectively. We note that the value of $z\nu$ lies in the range 4–12 whereas τ_0' is much slower than the range 10^{-12}–10^{-14} s for classical SG compounds [41]. Note that the values of τ_0' are typically found to be slower for the CG compound and nanoparticles exhibiting superspin-glass behavior than the classical SG compounds. The values of τ_0' of CG systems are $\sim 10^{-10}$ s for $La_{0.95}Sr_{0.05}CoO_3$ [12], $\sim 10^{-9}$ s for $LaMn_{0.7}Fe_{0.3}O_3$ [42] and $\sim 10^{-11}$ s for $CeNi_{0.5}Cu_{0.5}$ [43]. The slower values of the τ_0' have also been reported for interacting nanoparticles of α-Fe_2O_3 $\sim 10^{-9}$ s [44], $\sim 10^{-11}$ s [45] and $\sim 10^{-12}$ s [46]. In the case of amorphous Fe_2O_3 the value of τ_0' was reported to be $\sim 10^{-11}$ s [47]. The much slower values of τ_0' were also reported for diluted multilayer systems

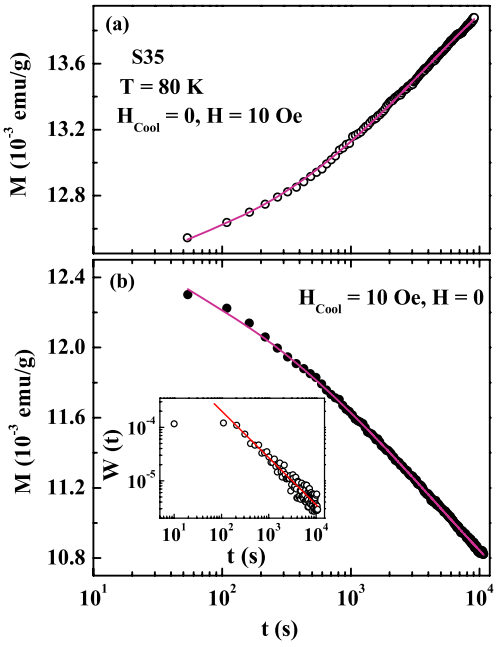

Figure 5. Time (t) dependence of magnetization (M) in (a) 10 Oe and (b) zero field which were cooled in ZFC and FC (10 Oe) modes, respectively, for S35. Inset of (b) shows the plot of $W(t)$ against t at 80 K. The solid lines exhibit the fit by power law decay, $W(t) = At^{-n}$. All experimental protocols are described in the text.

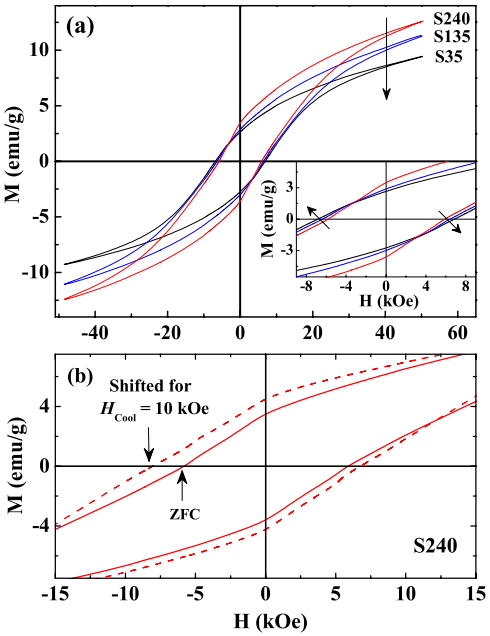

Figure 6. (a) Magnetic hysteresis loops at 5 K for S35, S135 and S240. Inset exhibits the central part of the loops. Arrows indicate the direction of decreasing grain size. (b) The shift in the central part of the hysteresis loop due to the field cooling is shown for S240.

$[Co_{80}Fe_{20}/Al_2O_3]$ in the range between $\sim 10^{-7}$ to 10^{-6} s, where τ_0' was decreased with the increase in dilution [48].

The time (t) dependence of magnetization was recorded at 80 K for S35 in two different experimental protocols. The sample was cooled down to 80 K from 250 K in zero (ZFC mode: cooling field, $H_{\rm cool} = 0$) and 10 Oe (FC mode: $H_{\rm cool} = 10$ Oe) and t evolution of magnetization was recorded at 80 K in 10 Oe and zero field, respectively. Time dependences measured in zero and 10 Oe field are shown in figures 5(a) and (b), respectively. Various functional forms have been proposed to describe the magnetization as a function of t. One of the most popular relations is the stretched exponential:

$$M(t) = M_0 - M_{\rm r} \exp[-(t/\tau_{\rm dc})^{\beta}] \qquad (3)$$

where M_0 and $M_{\rm r}$ are involved with the FM and exponential components, respectively. For classical SG systems M_0 is treated as 0 in equation (3) whereas a non-zero value of M_0 has been used for coexisting FM and SG components [13, 42, 49]. The relaxation process involves the activation against a single anisotropy barrier for $\beta = 1$ whereas β in the range, $0 < \beta < 1$ stands for the relaxation involved with the activation against the distribution of anisotropy barriers, typically found for SG compounds. Here, the term M_0 was required to fit the relaxation dynamics in both cases. The continuous curves in figures 5(a) and (b) exhibit satisfactory fits which yield the values of relaxation time ($\tau_{\rm dc}$) $\approx$ 3869 s and 4670 s with $\beta \approx$ 0.46 and 0.33, respectively. We further note that the values of the ratio $M_{\rm r}/M_0$ are $\approx$ 0.15 and $\approx$ 0.28 obtained from the fits displayed in figures 5(a) and (b), respectively. A considerable increase of $M_{\rm r}/M_0$ suggests a change in phase fraction due to the field-cooled effect where the glassy magnetic component increases and the FM component decreases as a result of field cooling.

The decay of the remanent magnetization with t in figure 5(b) was further fitted by the power law decay as $W(t) = At^{-n}$ after the lapse of a crossover time, t_0, where $W(t)$ is defined as $-(\mathrm{d}/\mathrm{d}t) \ln M(t)$ and A is a constant [50]. In order to explain the SG behavior of the FM nanoparticles, the above relation was proposed by Ulrich *et al* using Monte Carlo simulation with the assumption that the interparticle dipolar interaction has a distribution in grain size. They explicitly showed that decay of $M(t)$ follows the above relation with $n \geqslant 1$ for dense and $\approx 2/3$ for diluted or isolated FM nanoparticles. This theoretical model was recently corroborated by the relaxation of remanent magnetization for the spontaneously phase-separated manganites [51, 52] and cobaltites [13] in order to probe the strength of the interaction between FM clusters embedded in the non-FM matrix. The satisfactory fit of the t dependence of the remanent magnetization above $t_0 \approx 200$ s is shown in the inset of figure 5(b) by the solid straight line which gives the value of $n \approx 0.87$ at 80 K for S35. The value of n is close to the value observed in the bulk polycrystalline compound having slightly different composition, $La_{0.82}Sr_{0.18}CoO_3$ [13], indicating a moderate interaction between FM clusters.

3.2. Magnetic hysteresis and exchange bias effect

Magnetic hysteresis loops were measured at 5 K for S35, S135 and S240 which are displayed in figure 6(a). Magnetization does not show any saturating tendency at 50 kOe for all the samples in accordance with the previous reports where

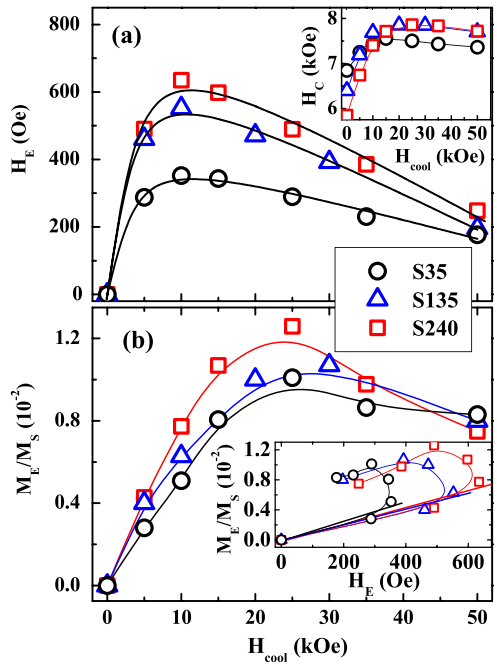

Figure 7. Cooling field ($H_{\rm cool}$) dependence of (a) EB field ($H_{\rm E}$) and (b) reduced EB magnetization, $M_{\rm E}/M_{\rm S}$, at 5 K for S35, S135 and S240. The $H_{\rm cool}$ dependence of coercivity ($H_{\rm C}$) are shown in the inset of (a). Plots of $M_{\rm E}/M_{\rm S}$ against $H_{\rm E}$ are shown in the inset of (b).

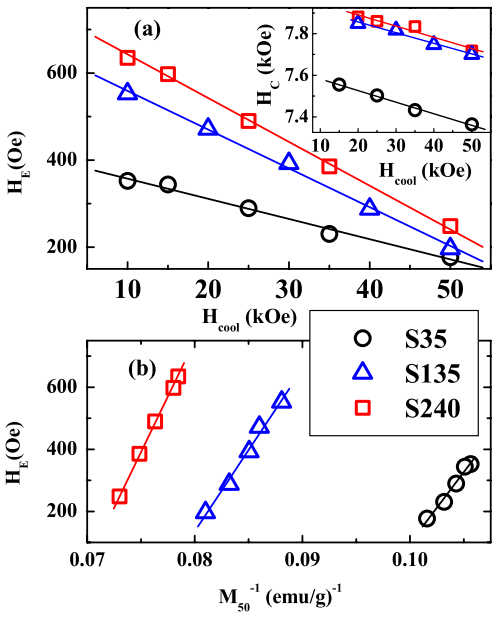

Figure 8. (a) Plots of exchange bias field ($H_{\rm E}$) against cooling field ($H_{\rm cool} \geqslant 10$ kOe) at 5 K for S35, S135 and S240. Inset shows the plot of $H_{\rm C}$ against $H_{\rm cool}$. (b) Plot of $H_{\rm E}$ as a function of the inverse of the average magnetization at 50 kOe (M_{50}^{-1}). Solid straight lines indicate the linear fits.

a significant fraction of the SG component gives rise to the non-saturating trend at high field [31, 32]. The magnetization at 50 kOe (M_{50}) and remanence magnetization increase considerably whereas coercivity ($H_{\rm C}$) decreases slightly (inset of figure 6(a)) with increasing grain size. The decrease of the fraction of the FM component is indicated by the decrease in M_{50} with decreasing grain size. When the sample was cooled down to 5 K from 250 K in a static field, the shifts in the hysteresis loops were observed for S35, S135 and S240. An example of the shift in the hysteresis loop at 5 K is shown in figure 6(b) for S240. The shifts of the hysteresis loops are the typical manifestations of the EB effect where the horizontal and vertical shifts are described as the EB field ($H_{\rm E}$) and EB magnetization ($M_{\rm E}$), respectively. The shifts at 5 K are estimated from the hysteresis loops measured in between $\pm$50 kOe at different $H_{\rm cool}$.

The $H_{\rm cool}$ dependence of $H_{\rm E}$ shown in figure 7(a) exhibits that initially, $H_{\rm E}$ increases sharply up to $H_{\rm cool} = 10$ kOe and then it decreases with further increase of $H_{\rm cool}$. $H_{\rm C}$ follows an almost similar $H_{\rm cool}$ dependence, which is shown in the inset of figure 7(a) for all the samples. Analogous to the $H_{\rm cool}$ dependence of $H_{\rm E}$ the values of $M_{\rm E}/M_{\rm S}$ follow a similar behavior with $H_{\rm cool}$ (figure 7(b)). $M_{\rm S}$ is the saturation magnetization which was determined from the extrapolation of the high-field magnetization at $1/H \rightarrow 0$. Recently, a simplified exchange interaction model has been proposed by Niebieskikwiat and Salamon considering the FM clusters embedded in an AFM host for a charge-ordered compound, $Pr_{1/3}Ca_{2/3}MnO_3$ [53]. The FM clusters were assumed to have a single domain structure like FM nanoparticles having a single magnetic domain embedded in the non-FM matrix. The model gives the simplified relation between $H_{\rm E}$ and $M_{\rm E}/M_{\rm S}$, $H_{\rm E} \propto M_{\rm E}/M_{\rm S}$ for $\mu H_{\rm E}/k_{\rm B}T < 1$, where μ is the average moment of the FM clusters. The linear dependence between $H_{\rm E}$ and $M_{\rm E}/M_{\rm S}$ has been verified in $Pr_{1/3}Ca_{2/3}MnO_3$ [53], $CaMnO_3$ [54], $LaMn_{0.7}Fe_{0.3}O_3$ [25, 37] and $Nd_{1-x}Sr_xCoO_3$ [38, 39]. The plots of $H_{\rm E}$ with $M_{\rm E}/M_{\rm S}$ are shown in the inset of figure 7(b). The plots exhibit nearly linear dependence up to $H_{\rm cool} = 10$ kOe, above which it deviates from the linearity. This happens due to the growth of FM clusters with increasing $H_{\rm cool}$ and μ increases associated with the increase in size of the FM clusters where $\mu H < k_{\rm B}T$ does not hold for $H_{\rm cool} \geqslant 10$ kOe. Furthermore, $H_{\rm E}$ (figure 8(a)) and $H_{\rm C}$ (inset of figure 8(a)) decrease linearly with $H_{\rm cool}$ above 10 kOe. We note that $H_{\rm E}$ decreases to $\approx 60\%$ for S135 and S240, whereas it decreases to $\approx 50\%$ for S35 with the increase of $H_{\rm cool}$ from 10 to 50 kOe. The growth of the FM clusters and decrease of $H_{\rm E}$ above $H_{\rm cool} = 10$ kOe are consistent with the model proposed by Meiklejohn which predicts the relation $H_{\rm E} \approx J_{\rm ex}/(M_{\rm FM} \times t_{\rm FM})$, where $J_{\rm ex}$ is the exchange constant across the FM/AFM interface per unit area [55]. $M_{\rm FM}$ and $t_{\rm FM}$ are the magnetization and thickness of the FM layer, respectively. The increase of $M_{\rm FM}$ associated with the increase of $t_{\rm FM}$ in the denominator of the above expression decreases the magnitude of $H_{\rm E}$. The decrease of $H_{\rm E}$ is consistent with the results of the exchange-biased systems having an SG component where the values of $H_{\rm E}$ decrease considerably with increasing $H_{\rm cool}$ in the high limit. $H_{\rm E}$ decreased to $\sim$47% for the increase of $H_{\rm cool}$ from 6 to 12 kOe in CG manganite, $LaMn_{0.7}Fe_{0.3}O_3$ [25, 37]. For CG cobaltite, $Nd_{0.88}Sr_{0.12}CoO_3$, $H_{\rm E}$ decreased to $\sim$22% for the increase of $H_{\rm cool}$ from 10 to 50 kOe [38]. For Fe and iron oxide core–shell nanostructures $H_{\rm E}$ decreased to 50% for the decrease of $H_{\rm cool}$ from 5 to 50 kOe, where iron oxide was reported to be in the disordered glassy magnetic state at low temperature [56, 57].

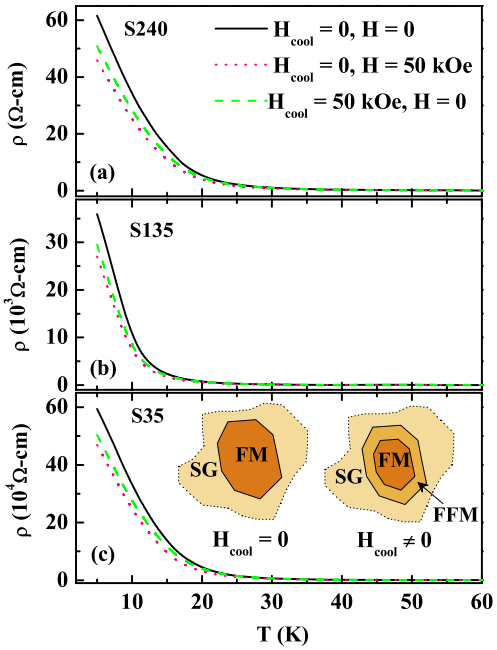

Figure 9. Temperature (T) dependence of resistivity (ρ) in zero-field (continuous curve), zero-field-cooled (ZFC) (dotted curve) and field-cooled (FC) (dashed curve) modes for S240 (a), S135 (b) and S35 (c) indicating the significant deviation from each other at low temperature. The cartoons of the interface region between the FM and SG components are proposed in the inset of (c) for different field-cooled modes.

Table 1. The percentage of $\rho_{EB} = (\rho_{FC} - \rho_{ZFC})/\rho_{ZFC}$ and MR $= (\rho_{ZFC} - \rho_0)/\rho_0$ at 6 K for different grain sizes.

Sample	ρ_{EB} (%)	MR (%)
S35	5.2	20.9
S135	8.9	24.9
S240	10.1	25.4

By taking into account that the magnetization at 50 kOe is close to the saturation magnetization, the values of M_{50} might be considered as proportional to the volume fraction of the FM component in the compound. Thus, an increase of M_{50} with increasing H_{cool} may indicate that the average size of FM clusters is enhanced due to the increase of H_{cool} for $H_{cool} > 10$ kOe. The values of H_E against $1/M_{50}$ are plotted in figure 8(b) for S35, S135 and S240. It is evident from the plots that the values of H_E are inversely proportional to M_{50}, i.e. average size of the FM clusters. We further note that the slope defined as $dH_E/d(M_{50}^{-1})$ increases with increasing grain size, indicating that the EB effect for the particles having the largest average size is more sensitive to the inverse of the saturation of magnetization or cooling field.

3.3. Transport properties

Semiconducting temperature dependence of resistivity (ρ) measured in the heating cycle under different cooling modes is shown in figure 9. In the case of the measurement of resistivity in ZFC and FC modes samples were cooled down to 5 K from 250 K in zero field and the cooling field ($H_{cool} = 50$ kOe),

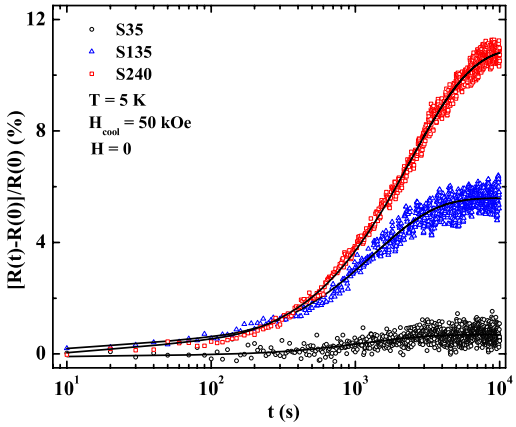

Figure 10. Time (t) dependence of the percentage of $[R(t) - R(0)]/R(0)$ is illustrated for S35, S135 and S240 where $R(0)$ is the resistance at $t = 0$. The continuous curve indicates the fit using the stretched exponential for S240.

respectively, and the temperature dependence was measured at 50 kOe field during warming up the samples. The values of ρ are found to increase considerably with decreasing grain size. The negative magnetoresistance (MR), defined as MR $= (\rho_{ZFC} - \rho_0)/\rho_0$, is observed below ~25 K where ρ_0 and ρ_{ZFC} are the resistivities in zero and static magnetic field cooled under ZFC conditions. The strong deviation between ZFC (ρ_{ZFC}) and FC (ρ_{FC}) resistivities at low temperature is observed where surprisingly the magnitude of $\rho_{FC}(T)$ is higher than $\rho_{ZFC}(T)$ for all the samples. The strong deviation between ρ_{ZFC} and ρ_{FC} was also reported by Wu *et al* for the single crystal of $La_{1-x}Sr_xCoO_3$ at $x = 0.15$ [16]. Here, we observe the similar behavior in the polycrystalline compound with slightly different composition at $x = 0.12$. Note that Wu *et al* suggested the glassy transport behavior of $La_{1-x}Sr_xCoO_3$ at the percolation threshold with $x = 0.18$ where they proposed the possible magnetoelectronic phase separation into nanoscale FM clusters embedded in a non-FM matrix to interpret the results. Here, we further suggest that the strong FC effect in ρ is correlated to the EB effect. When the sample is cooled in a static magnetic field ($H_{cool} \neq 0$), a new layer comprising of frozen FM (FFM) spins appears at the FM and SG interface. The cartoons at one of the interface regions between the FM and SG components are illustrated in the insets of figure 9(c) depending on the field-cooled modes. The appearance of FFM layers is described in the right inset of figure 9(c) which causes a higher value of ρ_{FC} than ρ_{ZFC} at low temperature. The values of $\rho_{EB} = (\rho_{FC} - \rho_{ZFC})/\rho_{ZFC}$ and MR $= (\rho_{ZFC} - \rho_0)/\rho_0$ at 6 K are shown in table 1 where both values decrease systematically with decreasing grain size. The decrease of ρ_{EB} is consistent with the decrease of H_E obtained from the magnetic hysteresis loop.

We further investigate the time dependence of resistance in different field-cooled modes. When samples were cooled in the ZFC mode and t evolution was recorded at 50 kOe, a very weak t dependence is observed for S240 which is absent for S135 and S35. On the other hand, a considerable t dependence in ρ is noticed while samples were cooled in the FC mode ($H_{cool} = 50$ kOe) and resistivity was recorded in zero field

after stabilizing the temperature at 5 K. The time dependence of $[R(t) - R(0)]/R(0)$ is displayed in figure 10 for S35, S135 and S240, where $R(0)$ is the resistance at $t = 0$. The results indicate that the observed time dependence due to the field cooling is correlated with the EB effect. We observe nearly $\approx$ 11% of the increase in resistance at $t = 10^4$ s compared to the value at $t = 0$ for S240 which are $\approx$ 5% and $\approx$ 1% for S135 and S35, respectively. In the case of glassy magnetic behavior t dependence of magnetization typically follows the stretched exponential [41]. We fit the t dependence of $[R(t) - R(0)]/R(0)$ using the stretched exponential, $R(t) = A + B\exp(-t/\tau_\rho)^\beta$ as described in equation (3), where τ_ρ is the relaxation time. The satisfactory fit of t dependence using a stretched exponential is shown by the continuous curve in the figure with $\tau_\rho = 2410$ s, 1353 s and 1200 s for S240, S135 and S35, respectively considering $\beta = 1$. Time dependence is weakened and τ_ρ is shortened considerably with decreasing grain size. We suggest that the observed time dependence is attributed to the appearance of the FFM layer. The fraction of the FFM layer decreases considerably with decreasing average grain size, resulting in the weak time dependence of resistivity.

In summary, nanocrystalline hole-doped cobaltite, $La_{0.88}Sr_{0.12}CoO_3$ is prepared by the sol–gel route using citrate precursor where sizes are varied from ~35 to ~240 nm. Analogous to that observed in the bulk counterpart, the nanocrystalline compound with average grain size ~35 nm exhibits the cluster-glass-like spin dynamics where short range ferromagnetic clusters still exist associated with the spin-glass component. The fraction of the ferromagnetic component decreases systematically with decreasing grain size. The signature of the exchange bias effect is shown both in the magnetic and transport properties where the exchange bias effect is weakened considerably due to the decrease in grain size. We propose that exchange bias is attributed to the appearance of a new frozen ferromagnetic layer at the ferromagnetic/spin-glass interface due to the field cooling. As a result of the decrease in grain size the overall area of the ferromagnetic/spin-glass interface as well as the fraction of frozen ferromagnetic spins have been reduced considerably, resulting in the weakening of the exchange bias effect. The strong field-cooled effect observed in the temperature and time dependences of resistivity is correlated to the appearance of frozen ferromagnetic spins which give rise to the exchange bias effect.

Acknowledgments

One of the authors (SG) wishes to thank the Department of Science and Technology, India (project no. SR/S2/CMP-46/2003) for the financial support. MP acknowledges the Council for Scientific and Industrial Research, India for the SRF fellowship.

References

[1] Wu J and Leighton C 2003 *Phys. Rev.* B **67** 174408
[2] Stauffer D D and Leighton C 2004 *Phys. Rev.* B **70** 214414
[3] Leighton C, Stauffer D D, Huang Q, Ren Y, El-Khatib S, Torija M A, Wu J, Lynn J W, Wang L, Frey N A, Srikanth H, Davies J E, Liu K and Mitchell J F 2004 *Phys. Rev.* B **79** 214420
[4] Asai K, Gehring P, Chou H and Shirane G 1989 *Phys. Rev.* B **40** 10982
[5] Yamaguchi S, Okimoto Y and Tokura Y 1997 *Phys. Rev.* B **55** R8666
[6] Zobel C, Kriener M, Bruns D, Baier J, Gruninger M, Lorenz T, Reutler P and Revcolevschi A 2002 *Phys. Rev.* B **66** 020402
[7] English S R, Wu J and Leighton C 2002 *Phys. Rev.* B **65** 220407(R)
[8] Caciuffo R, Rinaldi D, Barucca G, Mira J, Rivas J, Señarís-Rodríguez M A, Radaelli P G, Fiorani D and Goodenough J B 1999 *Phys. Rev.* B **59** 1068
[9] Wu J, Lynn J W, Glinka C J, Burley J, Zheng H, Mitchell J F and Leighton C 2005 *Phys. Rev. Lett.* **94** 037201
[10] Hoch M J R, Kuhns P L, Moulton W G, Reyes A P, Lu J, Wu J and Leighton C 2004 *Phys. Rev.* B **70** 174443
[11] Hoch M J R, Kuhns P L, Moulton W G, Reyes A P, Wu J and Leighton C 2004 *Phys. Rev.* B **69** 014425
[12] Nam D N H, Mathieu R, Nordblad P, Khiem N V and Phuc N X 2000 *Phys. Rev.* B **62** 8989
[13] Tang Y K, Sun Y and Cheng Z H 2006 *Phys. Rev.* B **73** 012409
[14] Nam D N H, Jonason K, Nordblad P, Khiem N V and Phuc N X 1999 *Phys. Rev.* B **59** 4189
[15] Mukherjee S, Ranganathan R, Anilkumar P S and Joy P A 1996 *Phys. Rev.* B **54** 9267
[16] Wu J, Zheng H, Mitchell J F and Leighton C 2006 *Phys. Rev.* B **73** 020404(R)
[17] Patra M, Majumdar S and Giri S 2009 *Europhys. Lett.* **87** 58002
[18] Dey P and Nath T K 2006 *Appl. Phys. Lett.* **89** 163102
[19] Dey P, Nath T K and Banerjee A 2007 *Appl. Phys. Lett.* **91** 012504
[20] Biswas A and Das I 2007 *Appl. Phys. Lett.* **91** 013107
[21] Biswas A, Das I and Majumdar C 2005 *J. Appl. Phys.* **98** 124310
[22] Biswas A and Das I 2006 *Phys. Rev.* B **74** 172405
[23] Sarkar T, Ghosh B, Raychaudhuri A K and Chatterji T 2008 *Phys. Rev.* B **77** 235112
[24] Rozenberg E, Shames A I, Auslender M, Jung G, Felner I, Sinha J, Banerjee S S, Mogilyansky D, Sominski E, Gedanken A, Mukovskii Ya M and Gorodetsky G 2007 *Phys. Rev.* B **76** 214429
[25] Thakur M, Patra M, De K, Majumdar S and Giri S 2008 *J. Phys. Condense Matter.* **20** 195215
[26] Zhang T and Dressel M 2009 *Phys. Rev.* B **80** 014435
[27] Huang X H, Ding J F, Zhang G Q, Hou Y, Yao Y P and Li X G 2008 *Phys. Rev.* B **78** 224408
[28] Markovich V, Fita I, Wisniewski A, Puzniak R, Mogilyansky D, Titelman L, Vradman L, Herskowitz M and Gorodetsky G 2008 *Phys. Rev.* B **77** 054410
[29] Fita I, Markovich V, Mogilyansky D, Puzniak R, Wisniewski A, Titelman L, Vradman L, Herskowitz M, Varyukhin V N and Gorodetsky G 2008 *Phys. Rev.* B **77** 224421
[30] Fuchs D, Pinta C, Schwarz T, Schweiss P, Nagel P, Schuppler S, Schneider R, Merz M, Roth G and Löhneysen H v 2007 *Phys. Rev.* B **75** 144402
[31] Tang Y K, Sun Y and Cheng Z H 2006 *Phys. Rev* B **73** 174419
[32] Tang Y K, Sun Y and Cheng Z H 2006 *J. Appl. Phys.* **100** 023914
[33] Huang W G, Zhang X Q, Du H F, Yang R F, Tang Y K, Sun Y and Cheng Z H 2008 *J. Phys.: Condens. Matter* **20** 445209
[34] Meiklejohn W H and Bean C P 1956 *Phys. Rev.* **102** 1413
[35] Nogues J and Schuller I K 1999 *J. Magn. Magn. Mater.* **192** 203

[36] Iglesias Ò, Labarta A and Batlle X 2008 *J. Nanosci. Nanotechnol.* **8** 2761
[37] Patra M, De K, Majumdar S and Giri S 2007 *Eur. Phys. J.* B **58** 367
[38] Patra M, Majumdar S and Giri S 2009 *Solid State Commun.* **149** 501
[39] Patra M, Thakur M, Majumdar S and Giri S 2009 *J. Phys.: Condens. Matter* **21** 236004
[40] De K, Ray R, Panda R N, Giri S, Nakamura H and Kohara T 2005 *J. Magn. Magn. Mater.* **288** 339
[41] Mydosh J A 1993 *Spin Glasses: An Experimental Introduction* (London: Taylor and Francis)
[42] De K, Patra M, Majumdar S and Giri S 2007 *J. Phys. D: Appl. Phys.* **40** 7614
[43] Marcano N, Gómez Sal J C, Espeso J I, Fernández Barquín L and Paulsen C 2007 *Phys. Rev.* B **76** 224419
[44] Parker D, Dupuis V, Ladieu F, Bouchaud J-P, Dubois E, Perzynski R and Vincent E 2008 *Phys. Rev.* B **77** 104428
[45] Fiorani D, Testa A M, Lucari F, D'Orazio F and Romero H 2002 *Physica* B **320** 122
[46] Winkler E, Zysler R D, Vasquez Mansilla M, Fiorani D, Rinaldi D, Vasilakaki M and Trohidou K N 2008 *Nanotechnology* **19** 185702
[47] Mukadam M D, Yusuf S M, Sharma P, Kulshreshtha S K and Dey G K 2005 *Phys. Rev.* B **72** 174408
[48] Kleemann W, Petracic O, Binek Ch, Kakazei G N, Pogorelov Yu G, Sousa J B, Cardoso S and Freitas P P 2001 *Phys. Rev.* B **63** 134423
[49] Thakur M, Patra M, Majumdar S and Giri S 2009 *J. Appl. Phys.* **105** 073905
[50] Ulrich M, Garcia-Otero J, Rivas J and Bunde A 2003 *Phys. Rev.* B **67** 024416
[51] De K, Patra M, Majumdar S and Giri S 2007 *J. Phys. D: Appl. Phys.* **40** 5810
[52] Rivadulla F, Lopez-Quintela M A and Rivas J 2004 *Phys. Rev. Lett.* **93** 167206
[53] Niebieskikwiat D and Salamon M B 2005 *Phys. Rev.* B **72** 174422
[54] Markovich V, Fita I, Wisniewski A, Puzniak R, Mogilyansky D, Titelman L, Vradman L, Herskowitz M and Gorodetsky G 2008 *Phys. Rev.* B **77** 054410
[55] Meiklejohn W H 1962 *J. Appl. Phys.* **33** 1328
[56] Del Bianco L, Fiorani D, Testa A M, Bonetti E and Signorini L 2004 *Phys. Rev.* B **70** 052401
[57] Fiorani D, Del Bianco L, Testa A M and Trohidou K N 2007 *J. Phys.: Condens. Matter* **19** 225007